The Biological Bulletin, February 2022, volume 242, number 1: 62–73. https://doi.org/10.1086/716711

Uncovering the Effects of Symbiosis and Temperature on Coral Calcification

ZOE DELLAERT[1], PHILLIP A. VARGAS[2], PATRICK J. LA RIVIERE[2], AND LORETTA M. ROBERSON[3,*]

[1]*Biological Sciences Collegiate Division and* [2]*Department of Radiology, University of Chicago, Chicago, Illinois 60637; and* [3]*Bell Center, Marine Biological Laboratory, Woods Hole, Massachusetts 02543*

Abstract. We tested the impact of temperature and symbiont state on calcification in corals, using the facultatively symbiotic coral *Astrangia poculata* as a model system. Symbiotic and aposymbiotic colonies of *A. poculata* were reared in 15, 20, and 27 °C conditions. We used scanning electron microscopy to quantify how these physiological and environmental conditions impact skeletal structure. Buoyant weight data over time revealed that temperature significantly affects calcification rates. Scanning electron microscopy of *A. poculata* skeletons showed that aposymbiotic colonies appear to have a lower density of calcium carbonate in actively growing septal spines. We describe a novel approach to analyze the roughness and texture of scanning electron microscopy images. Quantitative analysis of the roughness of septal spines revealed that aposymbiotic colonies have a rougher surface than symbiotic colonies in tropical conditions (27 °C). This trend reversed at 15 °C, a temperature at which the symbionts of *A. poculata* may exhibit parasitic properties. Analysis of surface texture patterns showed that temperature impacts the spatial variance of crystals on the spine surface. Few published studies have examined the skeleton of *A. poculata* by using scanning electron microscopy. Our approach provides a way to study detailed changes in skeletal microstructure in response to environmental parameters and can serve as a proxy for more expensive and time-consuming analyses. Utilizing a facultatively symbiotic coral that is native to both temperate and tropical regions provides new insights into the impact of both symbiosis and temperature on calcification in corals.

Received 17 March 2021; Accepted 4 July 2021; Published online 10 January 2022.

* To whom correspondence should be addressed. Email: lroberson@mbl.edu.

Abbreviations: FMP, first moment of the power spectrum; FSW, filtered seawater; ROI, region of interest; SEM, scanning electron microscopy.

Introduction

Many recent studies have examined the relationship between coral symbiosis and temperature in the context of coral bleaching, but few have examined the effects of symbiosis or temperature on the skeletal structure created by the coral. Most colonial corals contain photosynthetic symbionts within their gastrodermal tissues. These symbionts are unicellular dinoflagellates of the family Symbiodiniaceae (LaJeunesse *et al.*, 2018). They provide the coral with nutrients and are responsible for the brown or yellow colors of most tropical corals (Falkowski *et al.*, 1984). This relationship breaks down in a phenomenon known as coral bleaching (Baker *et al.*, 2018). In the tropics, high-temperature events associated with anthropogenic climate change trigger coral bleaching (Hughes *et al.*, 2003; Spalding and Brown, 2015; Heron *et al.*, 2016; van Hooidonk *et al.*, 2016). As the frequency of these high-temperature events increases (Hughes *et al.*, 2018), they could have long-lasting impacts on the relationship between corals and their symbionts as well as on the formation of the reef structure itself. The rate of calcification can be reduced up to 50% following a severe coral bleaching event (Lentz *et al.*, 2020). However, there is not yet a clear understanding of how bleaching might impact the structure of the skeleton. Any changes in the integrity or strength of the skeleton could increase susceptibility to storm damage or bioerosion, leading to further losses of coral cover.

The mechanism of calcification, which allows for the creation of the large reefs for which corals are known, is still not wholly understood (see reviews in Gattuso *et al.*, 1999; Allemand *et al.*, 2004, 2011; Tambutté *et al.*, 2011; Drake *et al.*, 2020). Calcification is the process by which reef-building corals create their calcium carbonate skeletons. Many previous studies have shown a relationship between light and calcification in symbiotic corals, known as diel or light-enhanced calcification

(LEC) (Goreau and Goreau, 1959; Moya *et al.*, 2006; Colombo-Pallotta *et al.*, 2010; Allemand *et al.*, 2011). However, whether the cause of light-enhanced calcification is due to the light itself, an intrinsic rhythmicity, or a secondary factor, such as the photosynthesis of the coral symbionts (symbiont-enhanced calcification), has been under debate for decades (Rinkevich and Loya, 1984; Moya *et al.*, 2006; Al-Horani *et al.*, 2007; Colombo-Pallotta *et al.*, 2010; Allemand *et al.*, 2011; Cohen *et al.*, 2016; Gutner-Hoch *et al.*, 2016). As a result of the persistent ambiguity surrounding the relationship between symbiosis and calcification, it is still largely unknown how widespread tropical coral bleaching will impact, and has already impacted, the calcification of tropical coral reefs. Corals can take 10 months to 2 years to fully recover from a bleaching event (Fitt *et al.*, 1993). During this time, the bleached colonies could have a very different pattern of calcification than non-bleached colonies. Changes in calcification that result from the repeated, more frequent bleaching events that have been predicted (Heron *et al.*, 2016), and now documented, in recent years will likely have a significant impact on coral survivorship and coral reef ecosystems.

The diel pattern of calcification was described in *Acropora cervicornis*, where deposition and growth of fusiform crystals occurred during both the night and day, while growth of acicular needles by increased accretion of calcium carbonate occurred only during the day (Gladfelter, 1983). This pattern is described as a laying down of scaffolding during the day and night, which is filled in by "bricks and mortar" during the day (Barnes and Crossland, 1980, p. 1116). Domart-Coulon *et al.* (2014) confirmed that linear extension rate was similar during the day and night and hypothesized that skeletal thickening is a separate mechanism from linear extension.

There is overwhelming evidence that symbiosis with Symbiodiniaceae can enhance calcification even if it is not the sole cause of increased calcification under light conditions (Allemand *et al.*, 2011; Drake *et al.*, 2020). There are two main hypotheses that could explain how photosynthesis by Symbiodiniaceae enhances coral calcification. One hypothesis is that the chemical environment created by the removal of carbon dioxide in photosynthesis creates a favorable equilibrium for aragonite precipitation (Goreau, 1959; Inoue *et al.*, 2018). The other main hypothesis is that photosynthates produced by the symbionts are transported to areas of active calcification where they are utilized in this process, possibly in the production of the organic matrix or as a supply of organic carbon for the formation of calcium carbonate itself (Pearse and Muscatine, 1971; Moya *et al.*, 2006, 2008; Bertucci *et al.*, 2015).

Research to date has not yet explored whether symbiotic state affects the morphology and structural integrity of the skeleton. If photosynthesis by Symbiodiniaceae does, for example, provide the coral with precursors for skeletal organic matrix proteins (Moya *et al.*, 2008) or somehow enhances the aragonite saturation state at the calcifying site (Inoue *et al.*, 2018), the size and shape of the skeleton may be affected by the breakdown or absence of symbiosis. Most data regarding symbiont-enhanced calcification draw conclusions based on calcification rate data. Few studies have taken the approach of examining the effect of symbiont state on the underlying calcification patterns themselves.

In the past, experiments studying the effect of symbiosis on coral calcification have been performed only on tropical corals, which are either obligately symbiotic or exclusively asymbiotic. Early studies on *Manicina areolata* and *Oculina diffusa* showed that calcification was depressed in the absence of endosymbionts (Goreau, 1959). In experiments comparing the calcification of the symbiotic coral *Galaxea fascicularis* with that of asymbiotic *Tubastrea faulkneri*, it was found that the rate of calcium incorporation was the same for the two species in control conditions (Marshall, 1996). However, when photosynthesis was inhibited by the introduction of Diuron (DCMU [3-(3,4-dichlorophenyl)-1,1-dimethylurea]), calcification was repressed in symbiotic *Galaxea* and unaffected in asymbiotic *Tubastrea* (Marshall, 1996). Other work describing the difference between symbiotic and asymbiotic coral species has described differences in Ca^{2+} uptake, skeletal organic matrix composition, and skeletal density banding (Gautret *et al.*, 1997; Clode and Marshall, 2004; Frankowiak *et al.*, 2016). Moya *et al.* (2008) characterized the calcification of microcolonies of *Stylophora pistillata* following a pollution event that caused bleaching and found a significant decrease in both light and dark calcification rates following the breakdown of symbiosis. However, the extreme stress of such a bleaching event makes it difficult to directly link this decrease in calcification rate to the loss of symbionts. An experiment utilizing *Montastraea faveolata* found a similar reduction in calcification in bleached colonies that could be rescued by the addition of oxygen (Colombo-Pallotta *et al.*, 2010). Other recent studies have examined the calcification of *Acropora digitifera* in an aposymbiotic state in the primary polyp phase, reared from larvae in the absence of Symbiodiniaceae. These authors found that aposymbiotic polyps had an altered macro-scale skeletal structure and decreased calcification rate relative to symbiotic primary polyps (Iwasaki *et al.*, 2016; Inoue *et al.*, 2018). These experiments all suggest that in symbiotic corals, photosynthesis is tightly linked to calcification rate. However, all of them compared obligately symbiotic species with asymbiotic tropical species or utilized symbiotic tropical corals in a non-symbiotic stressed state. Therefore, these studies could not determine whether the diel pattern of calcification was due solely to symbiotic state and not another factor, such as circadian rhythm, metabolic rates, or species-level differences.

Astrangia poculata provides a way to independently study the role of symbiosis and the impact of temperature on skeleton formation in tropical corals. This model species is a scleractinian coral whose large geographical range extends from the tropical Caribbean to temperate Cape Cod, Massachusetts (Peters *et al.*, 1988). *Astrangia poculata* exhibits a facultative symbiotic relationship with *Breviolum psygmophilum* (LaJeunesse

et al., 2012). Unlike most tropical corals, *A. poculata* has the ability to survive in both symbiotic and aposymbiotic states (Peters *et al.*, 1988). Additionally, *A. poculata* can uniquely survive in a large range of temperatures (~0–30 °C) (Dimond *et al.*, 2013). *Astrangia poculata* forms a skeleton, which sets it apart from the sea anemone *Exaiptasia pallida*, which is a commonly used coral model system. This coral species maintains a large range of photosymbiont densities (Sharp *et al.*, 2017), and the larger symbiont density values are comparable to densities in tropical coral species (Table 1). Because of its hardiness and naturally wide temperature range, *A. poculata* is also easy to culture in a laboratory setting at a wide range of temperatures.

Here we employ novel roughness and texture analyses to take a detailed look at the microstructure of symbiotic and aposymbiotic *A. poculata* skeletons, to assess the impacts of both symbiosis and temperature on calcification. In this study, we use scanning electron microscopy (SEM) to visualize structural patterns of active calcification in the presence and absence of symbionts under three different temperatures reflecting the range experienced by *A. poculata*. By quantifying the roughness and texture of coral skeleton surfaces in SEM images, we utilize the microstructure of the skeletons to better understand the role of symbionts in the skeletal thickening with bricks and mortar. Our approach provides a way to study detailed changes in skeletal microstructure in response to environmental parameters and can serve as a proxy for more expensive and time-consuming analyses, such as NanoSIMS (Nanoscale secondary ion mass spectrometry; CAMECA, Gennevilliers, France). We hypothesize that if symbionts determine calcification patterns, these patterns will differ in aposymbiotic and symbiotic states, mirroring the diel pattern of calcification found in symbiotic tropical corals. We expect that temperature will increase the rate of calcification as metabolic rates increase. Finally, we hypothesize that temperature and symbiont state will interact such that the effect of symbiont state on skeletal structural patterns will differ at the highest and lowest temperatures tested.

Table 1

Mean symbiont density (no. cm^{-2}) ± standard error of aposymbiotic and symbiotic Astrangia poculata *colonies at three study temperatures at the end of the experimental treatment*

Temperature (°C)	Aposymbiotic	Symbiotic
15	Below detection	$4.37 \times 10^5 \pm 4.24 \times 10^4$
20	Below detection	$7.26 \times 10^5 \pm 9.21 \times 10^4$
27	$5.57 \times 10^3 \pm 2.61 \times 10^3$	$3.86 \times 10^5 \pm 8.86 \times 10^4$
Astrangia poculata[a]	1×10^4–1×10^6	$>1 \times 10^6$
Montastrea annularis[b]	$2.7 \times 10^5 \pm 2.0 \times 10^5$	$1.08 \times 10^6 \pm 3.4 \times 10^5$

Published symbiont densities for *A. poculata* and *M. annularis* are included for comparison.

[a] Symbiont density data of aposymbiotic and symbiotic *A. poculata* colonies measured by alternative technique (Sharp *et al.*, 2017).

[b] Symbiont density data of bleached (light-colored) and unbleached (dark-colored) *M. annularis* colonies used for comparison (Fitt *et al.*, 1993).

Materials and Methods

Coral husbandry

We collected a total of 36 *Astrangia poculata* (Ellis & Solander, 1786) colonies (18 symbiotic and 18 aposymbiotic), 1–2 cm in diameter, from the Marine Biological Laboratory and Woods Hole Oceanographic Institution docks in Woods Hole, Massachusetts, using scuba. Six of each type were kept in three different common garden settings that represent the range of temperatures experienced by *A. poculata*: 15, 20, or 27 °C filtered seawater (FSW). These colonies were acclimated to their treatment temperatures for at least one month before the initial buoyant weight measurement. The experimental treatment period lasted 32 days. During this time, we fed the colonies freshly hatched *Artemia* sp. nauplii three times per week and maintained them at their experimental temperatures. Colonies were maintained in flow-through seawater systems and light levels of 20 μmol photons m^{-2} s^{-1} under an ambient light:dark cycle. We reared the colonies and imaged them using SEM in the same conditions as described above, but these were acclimated to their respective temperatures for at least three months prior to imaging.

Symbiont density analysis

Measurements of endosymbiotic density were taken before and after experimental treatment, using a non-destructive method to confirm symbiont status. We took 2 images of about 1 mm^2 of oral disk tissue for 2 polyps per colony, using a Zeiss Axio Zoom V16-2 stereo microscope (Oberkochen, Germany). Then, using the cell counter function of ImageJ software (https://imagej.nih.gov/ij/index.html), we counted the amount of symbiont cells in these images and calculated the average symbiont density for each colony as number of cells per square centimeter.

Calcification measurement

Buoyant weight was measured at the beginning and end of the 32-day period to determine calcification rates, using the method of Jokiel *et al.* (1978). We placed coral samples on a platform attached to a hook on an analytical balance (Sartorius Practum 64-1S, Goettingen, Germany) to weigh the corals while they remained submerged in FSW. Calcification rate was calculated as percent change per day to control for variation in colony size.

Calcein staining and imaging

We used calcein to identify active sites of calcification to be used in the image analysis. Live coral samples were stained

in 50 mL of a 20 μmol L^{-1} calcein solution for 13 hours to identify active calcification sites. Staining was performed in the dark. We imaged prepared skeletons, using a Zeiss Axio Zoom V16-2 stereo microscope with a GFP fluorescence filter. Calcein staining revealed that in most colonies, active calcification occurred on septa near the rim of the calyx (Fig. 1D).

Preparation of skeletons for scanning electron microscopy

Coral samples were anesthetized in a 0.185 mol L^{-1} $MgCl_2$ solution to facilitate excess tissue removal. Samples were then placed in a 1:1 solution of deionized (DI) water and commercial bleach (5% NaOCl) for 1 hour and then air dried (Fig. 1B, C). We cut the skeletons by using a bandsaw to remove a small sample of about five polyps for SEM imaging. All samples were prepared midday.

Scanning electron microscopy

Skeletons were sputter coated with platinum of roughly 10-nm thickness, using a Leica EM MED020 Cryo prep, sputter, and evaporative coater (Leica Microsystems, Buffalo Grove, IL). These were imaged using a Zeiss Supra 40VP scanning electron microscope at 5 kV. Corals were imaged at the tips of septa to locate sites of active growth based on the patterns seen in calcein staining (Fig. 1E–H). For quantitative analysis, two colonies were selected for SEM imaging per condition, and two to four polyps were imaged per colony. For each polyp 2 to 7 septa were imaged, resulting in about 20 septal spine images per condition.

Quantitative analysis of skeletal structure

Image selection criteria. In order to be used for quantitative analysis, images were selected only if the septal spine was clearly in focus. Certain samples displayed defects from inevitable sample preparation limitations, such as thick pooling of sputter coating or obvious cracks in the coating where organic material may not have been fully removed. Images for which such defects obscured the plane of analysis were not used. Septal spine images containing such defects outside of the analysis plane were still used, but those areas were excluded from the analysis by using masks.

Image normalization. Images underwent normalization in order to allow us to compare the pixel intensities across images. Prior to roughness analysis, images were combined into a stack in ImageJ. The images were normalized to each other by using the Enhance Contrast feature, with a saturated pixel value of 0.3%, using the stack histogram to equalize the histograms of the images.

Roughness analysis. For each image, 10 parallel line segments of 2.5 μm were drawn perpendicular to the axis of the septal spine (Fig. A1). A two-dimensional graph of the pixel intensities of each line segment was created using the Plot Profile function in ImageJ (Fig. A1). The pixel intensity graph serves as a proxy for the geometry of the cross section of

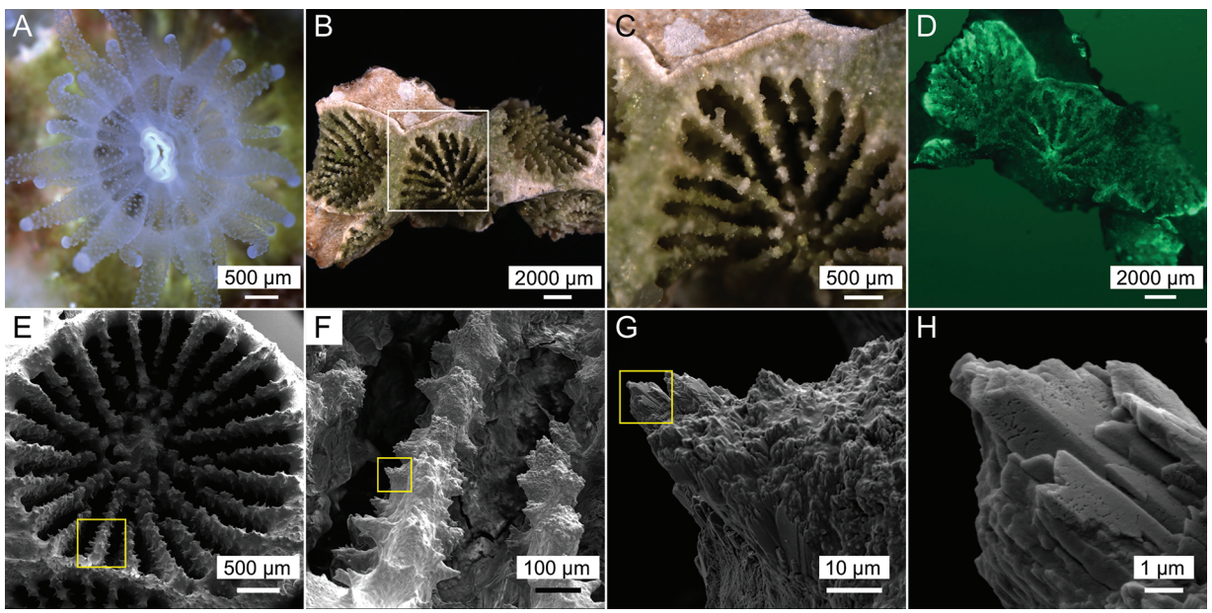

Figure 1. Sampling *Astrangia poculata* for scanning electron microscopy (SEM) imaging for texture and roughness analysis. (A) Live aposymbiotic *A. poculata* polyp. (B, C) Skeleton with tissue removed. (C) is an enlargement of (B), indicated by the box in (B). (D) Skeleton showing fluorescent calcein staining displaying sites of active calcification on septa. (E) SEM image of skeletal calyx. (F–H) Magnification of (E). (H) represents scale of images used for roughness and texture analysis.

crystals along that line segment. Bright areas with high intensity correspond to the face of the crystal; dark areas with lower intensities correspond to the edges of crystals (Fig. A2). These data were then converted into a time series in RStudio (ver. 1.2.1114, RStudio, 2018) to utilize frequency analyses to identify the dominant frequency or, in this case, the bumpiness of the skeleton surface, to generate a roughness value. We calculated roughness using the seewave package in RStudio. Briefly, roughness for each profile was calculated from the total curvature (roughness = Σ(second derivative^2)) (Sueur *et al.*, 2008). These 10 roughness values were averaged for each image to generate a roughness value per sample.

Texture analysis. Images were normalized using adaptive equalization to normalize the histograms of the images so that any differences in image intensities would be controlled for in the analysis. Normalization was performed using the exposure .equalize_adapthist function from the scikit-image library in Python (Walt *et al.*, 2014). Then a mask of each image was created to identify the foreground of the image and to remove any image defects from the data analyzed. The mask was divided into 200 pixel × 200 pixel regions of interest (ROIs). There were 1–1248 complete ROIs per image, but the majority of images had about 200 ROIs. The first moment of the power spectrum (FMP) was calculated for each ROI, using a two-dimensional Fourier transform (see Figs. A1, A3); these were averaged for each image. These represent the dominant frequencies in the calcification pattern.

Statistical analysis of data

Data were analyzed using GraphPad Prism version 9.0.2 for macOS (GraphPad Software, San Diego, CA).

Calcification rates. We used simple linear regression to analyze the calcification rates against temperature.

Roughness and texture measurements. We used two-way ANOVA, followed by Tukey's multiple comparisons *post hoc* test, to analyze the effect of temperature and symbiont state on roughness and texture. Roughness and texture data were transformed using $\log_{10}$ and inverse transformations, respectively, to satisfy the assumptions of ANOVA. As mentioned above, 2 colonies were selected for SEM imaging per condition (temperature and symbiont state), resulting in about 20 septal spine images per condition. We compared the mean measured values between the colonies in each condition and found no significant difference for roughness or texture, except for the aposymbiotic 27 °C colonies (unpaired *t* test on transformed data). For both the roughness and texture measurements, the mean of the values from one aposymbiotic 27 °C colony (AH1) was higher than the mean of the other (AH2). However, no outliers were found (ROUT function, Prism version 9.0.2 for macOS, GraphPad Software), so the values were still included in the analysis. All assumptions of two-way ANOVA were met. This allowed us to pool samples and report data by condition, with each individual data point representing one image analyzed.

Results

Symbiont state characterization

The symbiont densities at the end of the experimental treatment are reported in Table 1. Symbiont density remained stable throughout the experiment, and a simple *t* test within each group revealed that there was no significant difference between the initial and final values for any condition group. For aposymbiotic corals reared at 15 °C and 20 °C, the symbiont density was below detection at both time points. At the highest temperature, photosymbiont cells were detected in the aposymbiotic colonies, but the cell densities were two orders of magnitude lower than symbiotic counterparts (Table 1). The symbiont densities measured for both aposymbiotic and symbiotic colonies at all temperatures were lower than the range of densities found in colonies of *Astrangia poculata* at corresponding temperatures by Sharp *et al.* (2017) and may reflect the non-destructive method used in this study, which cannot detect symbiont cells deeper in the colony. Symbiont densities were also comparable to, but generally lower than, published symbiont densities of bleached and unbleached tropical corals (Table 1; Fitt *et al.*, 1993).

Temperature affects the rate of calcification

Calcification rate increased significantly with temperature for symbiotic ($F_{1,17} = 18.34$, $R^2 = 0.5190$, $P = 0.0005$) and aposymbiotic ($F_{1,15} = 8.823$, $R^2 = 0.3704$, $P = 0.0095$) colonies (Fig. 2). Symbiont state did not affect calcification rates. Calcification rates ranged from 0.096 to 1.2 mg aragonite d^{-1}. As shown in Figure 2, some colonies lost mass over the course of the experiment, up to −3.3 mg aragonite d^{-1}.

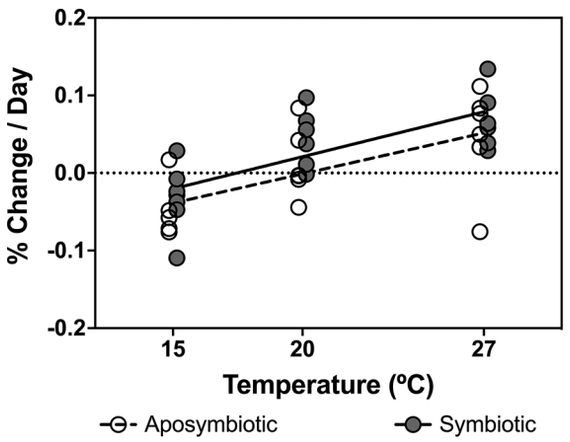

Figure 2. Calcification rate of *Astrangia poculata* measured using the buoyant weight technique. Calcification of *A. poculata* is significantly enhanced by increased temperature for symbiotic ($F_{1,17} = 18.34$, $R^2 = 0.5190$, $P = 0.0005$) and aposymbiotic ($F_{1,15} = 8.823$, $R^2 = 0.3704$, $P = 0.0095$) colonies. Lines indicate significant regression (slope different from zero).

Symbiont state and temperature interact to determine calcification structural patterns

Analysis of calcification structural patterns reveals not only that there is a relationship between the rate of calcification and temperature, as shown previously, but also that temperature has the ability to affect the structural pattern of calcification. In aposymbiotic colonies, septal spine roughness increased significantly with temperature (Fig. 3). In symbiotic colonies, however, roughness decreased with temperature (Fig. 3).

Our analysis also reveals a relationship between calcification structural patterns and symbiont state. A qualitative difference in the skeletal surface can be observed when comparing aposymbiotic and symbiotic colonies at 27 °C (Fig. 4). In colonies reared at 27 °C, the skeletal surfaces of aposymbiotic septal spines were significantly rougher than in symbiotic colonies (Fig. 3). Interestingly, this trend was reversed in colonies reared in cold water (15 °C). At this temperature, symbiotic colonies had a skeletal surface that was significantly rougher than that of aposymbiotic colonies (Fig. 3). By two-way ANOVA (Table 2), the interaction between temperature and symbiont state was significant and accounted for 18% of the total variance in the roughness dataset ($F_{2, 127} = 14.34$, $P < 0.0001$).

We found that the texture of septal spines was the same for all colonies except for symbiotic colonies reared at 27 °C (Fig. 5). By two-way ANOVA (Table 2), surface texture measured using FMP varied significantly in response to the interaction between temperature and symbiont state ($F_{2, 127} = 4.44$, $P = 0.0137$). The surface texture metric is based on the characteristic size of pattern features on septal spine surfaces in the entire region of interest, as opposed to the linear segments analyzed for the roughness measurement.

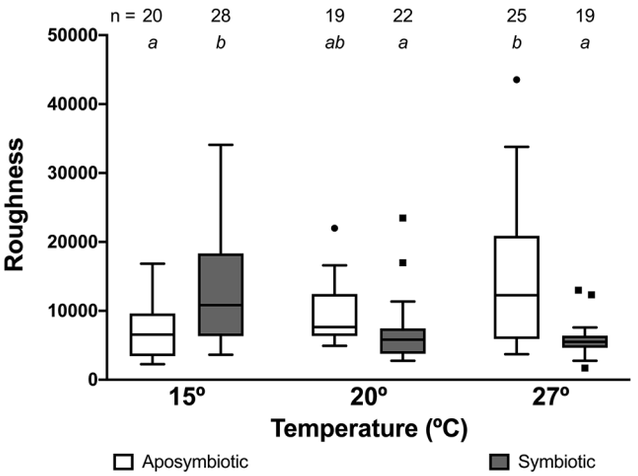

Figure 3. Roughness of septal spines of *Astrangia poculata*. At 27 °C, septal spines of aposymbiotic *A. poculata* colonies were significantly rougher than those of symbiotic colonies. This trend was reversed at 15 °C, where symbiotic septal spines are significantly rougher than aposymbiotic ones. There was no significant difference between aposymbiotic and symbiotic spines at 20 °C. The interaction between temperature and symbiont state accounts for 18% of the total variance ($F_{2, 127} = 14.34$, $P < 0.0001$). Lowercase letters above boxes indicate significant differences between groups by Tukey's *post hoc* test ($P < 0.05$).

Discussion

This study demonstrates that calcification in *Astrangia poculata* is affected by both temperature and symbiotic state. We found that the patterns of calcification revealed by SEM were significantly altered by both temperature and the presence or absence of symbionts. The rate of calcification, however, was enhanced by temperature. Dimond *et al.* (2013) found that the upper latitudinal limit of *A. poculata* was determined by temperature; growth is limited below 10 °C. Based on these results, we predicted that calcification rates of all individuals would increase with temperature as metabolic and growth rates increased (Marshall and Clode, 2004; Dimond *et al.*, 2013). Our results confirmed those of a previous study that found that temperature enhanced the calcification of symbiotic and aposymbiotic *A. poculata* (Jacques *et al.*, 1983). Jacques *et al.* (1983) also found evidence for symbiont-enhanced calcification under light conditions; in dark conditions there was no difference in calcification rates between symbiotic and aposymbiotic *A. poculata* colonies. We were unable to corroborate these findings because we measured net calcification over a 32-day time period and did not directly measure the calcification rate during the day and night. However, our analysis of skeletal surface roughness does suggest a difference in the structural pattern of calcification between aposymbiotic and symbiotic colonies of *A. poculata*.

In colonies reared in warm conditions, the absence of symbionts resulted in septal spines with a structure resembling flimsy scaffolding, as described in the pattern of night calcification of *Acropora cervicornis* (Barnes and Crossland, 1980; Gladfelter, 1983). This result provides data for a previous observation of the resemblance between aposymbiotic *A. poculata* skeletons and the nighttime skeletons of *Porites* (Cohen *et al.*, 2002; Cohen and McConnaughey, 2003). Symbiotic skeletons appeared to have the bricks and mortar that the aposymbiotic colonies lacked. However, it should be noted that calcification clearly takes place in aposymbiotic *A. poculata* even in the absence of symbionts.

We suggest that the in-filling or thickening aspect of calcification is enhanced by symbiont presence and is greatly reduced in aposymbiotic colonies at 27 °C. Chan *et al.* (2021) found that dark respiration of *A. poculata* was higher for symbiotic colonies than aposymbiotic colonies at all temperatures. Symbiotic corals at 27 °C may have higher levels of respiration stemming from both heterotrophically and autotrophically acquired sugars and have an increased photosynthate supply for the thickening of skeletal deposits. Aposymbiotic colonies reared at 27 °C may perform only the basal mechanism of calcification or linear extension (Goreau, 1959; Moya *et al.*, 2008). This could be explained by a reduced supply of inorganic carbon

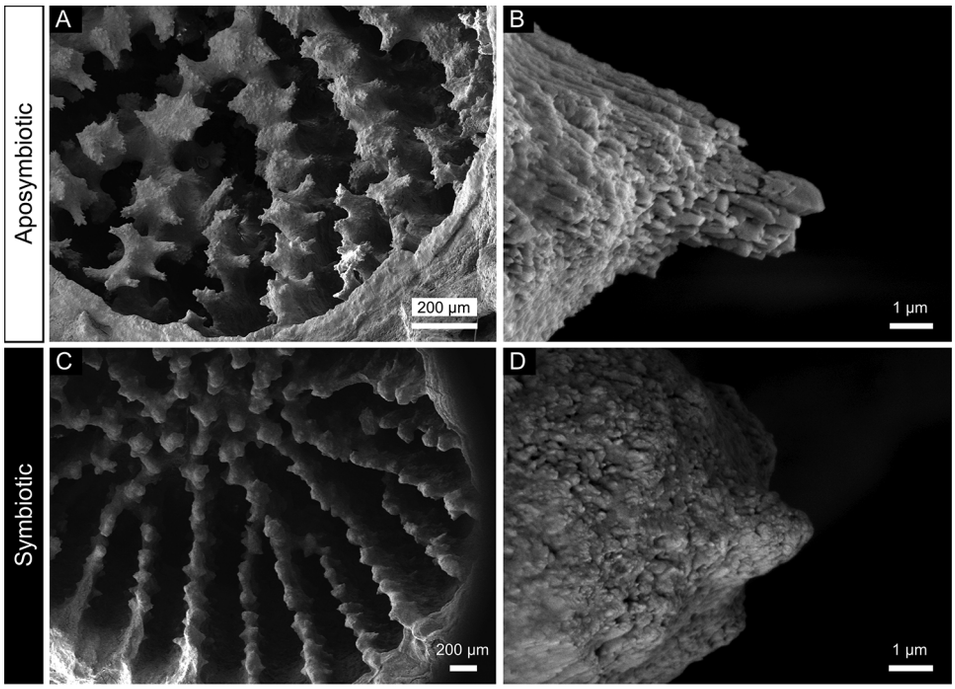

Figure 4. Scanning electron microscopy (SEM) imaging of *Astrangia poculata* skeleton. Qualitative differences in skeletal structure of aposymbiotic (A, B) and symbiotic (C, D) colonies of *A. poculata* reared at 27 °C. The septal protrusions of aposymbiotic colonies appear to be sharp and unfinished (A). In symbiotic colonies (C), the septa instead have rounded protrusions. These differences are mirrored when comparing aposymbiotic and symbiotic septa on a micro scale, at the level of septal spines (B, D). In these sites of active calcification, SEM revealed that septal spines of aposymbiotic corals at 27 °C (B) have more exposed large crystals compared to septal spines of symbiotic colonies (D). The surfaces of septal spines of symbiotic colonies at 27 °C (D) are composed of smaller crystals and are therefore smoother than aposymbiotic septal spines.

from respiration stimulated by the photosynthesis of the symbionts (Frankowiak *et al.*, 2016).

Alternatively, symbiont-enhanced calcification at 27 °C could be attributed to the supply of organic matrix precursor molecules (Moya *et al.*, 2006) by the photosynthesis of *Breviolum psygmophilum*, which is highest at this temperature (Chan *et al.*, 2021). A study comparing gene expression of *Acropora millepora* during the day and night found that light conditions were associated with increased expression of organic matrix-associated genes (Bertucci *et al.*, 2015). In this case, aposymbiotic *A. poculata* could have an altered skeletal organic matrix composition compared to symbiotic *A. poculata* (Frankowiak *et al.*, 2016). Organic matrix molecules such as coral acid-rich proteins (CARPs) are likely responsible for the stabilization of amorphous calcium carbonate particles in early stages of calcification (Bhattacharya *et al.*, 2016; Mass *et al.*, 2016; Von Euw *et al.*, 2017; Neder *et al.*, 2019). Moynihan *et al.* (2021) found that environmental parameters were reflected in

Table 2

Two-way ANOVA tables for roughness and texture measurements of scanning electron microscopy images of the Astrangia poculata *skeletal surface at septal spines*

	Roughness				Surface texture			
Source	df	%	*F*	*P*	df	%	*F*	*P*
Interaction	2	17.72	14.34	<0.0001	2	5.934	4.438	0.0137
Temperature	2	0.6874	0.5563	0.5747	2	6.988	5.226	0.0066
State	1	2.784	4.505	0.0357	1	3.321	4.967	0.0276
Residual	127				127			

df, degrees of freedom.

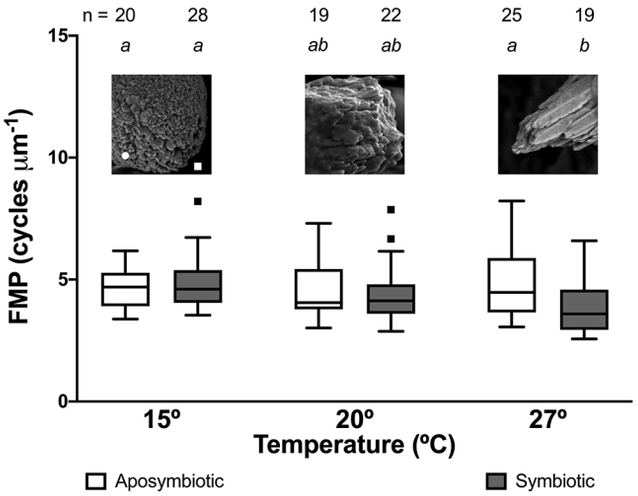

Figure 5. Surface texture of septal spines of *Astrangia poculata*. Surface texture is quantified by the metric first moment of the power spectrum (FMP) in cycles per micrometer. The interaction between temperature and symbiont state accounts for 6% of the total variance ($F_{2, 127} = 4.44$, $P = 0.0137$). Temperature alone accounts for 7% of the total variance ($F_{2, 127} = 5.23$, $P = 0.0066$). Symbiont state alone accounts for 3% of the total variance ($F_{1, 127} = 4.97$, $P = 0.0276$). Lowercase letters above boxes indicate significant differences between groups by Tukey's *post hoc* test ($P < 0.05$). The only statistically significant comparisons were between 15 °C aposymbiotic, 15 °C symbiotic, 27 °C aposymbiotic, and 27 °C symbiotic spines. As indicated by the example images, corals reared at 15 °C tended to have septal spines with small crystals that were close together, resulting in high FMP values compared to corals grown at higher temperatures.

the organic content of the skeletons of *Porites* spp. corals, which resulted in altered skeletal mechanical properties. If the organic matrix of aposymbiotic *A. poculata* is of a different composition than its symbiotic counterpart, the pattern of aragonite precipitation could be affected. This may be reflected in the mechanical properties of the skeleton and in the outermost skeletal surface. By either hypothesis, the lack of photosynthesis results in the altered skeletal structure as seen in this study.

By the roughness of septal spines, the pattern of calcification of *A. poculata* is different when raised in cold temperatures compared to warm temperatures. Roughness analyses revealed that structural patterns of calcification in colonies reared in cold water were reversed from those seen at warm temperatures. At warmer temperatures, the skeletons of aposymbiotic colonies were rougher, but at cold temperatures, symbiotic colonies had rougher skeletons. This reversal in trend could be due to increased dissolution of the aragonite skeleton at colder temperatures, where aragonite dissolution is favored (Burton and Walter, 1987). At warm temperatures below a certain upper limit that varies by species, Symbiodiniaceae have a higher rate of photosynthesis (Jacques *et al.*, 1983; Chan *et al.*, 2021). *Breviolum psygmophilum*, the symbiont found in association with *A. poculata*, reaches its maximum photochemical efficiency at 27 °C (Chan *et al.*, 2021). Both the rate and efficiency of photosynthesis decrease below this temperature. Jacques *et al.* (1983) showed that the presence of symbionts did not enhance the rate of calcification of *A. poculata* at temperatures at or below 15 °C. It has been suggested that the symbionts of *A. poculata* may become parasitic at low temperatures (Dimond and Carrington, 2008; Dimond *et al.*, 2013). At 15 °C, *B. psygmophilum* may stop photosynthesizing and become heterotrophic, scrounging the coral's resources (Dimond and Carrington, 2008; Thornhill *et al.*, 2008; Chan *et al.*, 2021). This helps explain the observed seasonal shifts in symbiont densities of *A. poculata*, which has been found to become paler during winter months (Dimond and Carrington, 2008; Sharp *et al.*, 2017). While cold-induced paling was not observed in our study, we hypothesize that the negative repercussions of maintaining a high symbiont density at cold temperatures may be the cause of the difference in skeletal surface roughness of aposymbiotic and symbiotic colonies of *A. poculata* at 15 °C.

The surface texture analysis quantitatively confirms the trend that *A. poculata* raised at cold temperatures deposits calcium carbonate with a different structural configuration than at warm temperatures. The FMPs for all groups other than symbiotic corals at 27 °C were not significantly different from one another. Therefore, the texture of septal spines for both aposymbiotic and symbiotic colonies at 15 °C and 20 °C is similar to that of aposymbiotic colonies reared at 27 °C. As mentioned in the previous paragraph, the thermal optimum of *B. psygmophilum* is around 27 °C (Chan *et al.*, 2021). Below its thermal optimum, *B. psygmophilum* may not provide a large enough advantage to *A. poculata* to be reflected in the surface texture of the septal spines. This is seen in Figure 5, in which the presence of symbionts at 15 °C and 20 °C does not significantly change the surface texture.

While the roughness analysis was able to reveal a difference in calcification patterns between aposymbiotic and symbiotic colonies at 15 °C, the texture analysis did not. The FMP metric is a measure of the frequency content of a textured pattern (Chinander *et al.*, 1999; Li *et al.*, 2005). A metric based on texture frequency, while more commonly used in biological image analysis, is not able to capture the same magnitude of differences of amplitude and crystal arrangement as the roughness method. The 27 °C symbiotic group was found to have the lowest FMP value of all, which may reflect the rapid growth by symbiotic colonies at this temperature. This analysis supports the results of the roughness analysis in confirming that the temperature of the environment has an effect on the calcification pattern of *A. poculata*. Analysis of skeletal surface can tell only so much of the story, and methods such as micro-computed tomography (micro-CT) and materials analysis will be needed to completely elucidate the role of temperature and symbiosis on the underlying skeletal strength and structure.

We studied symbiont-enhanced calcification in *A. poculata*, a facultatively symbiotic coral, and found that the pattern, but not the rate, of calcification is determined by symbiont state and temperature. Calcification rate, however, is enhanced by temperature alone. Our analysis of the microstructure of this

coral's skeleton reveals a complex interplay between symbiosis and temperature: the benefits of mutualism exist on a sliding scale that is dictated by environmental parameters. While the endosymbionts of *A. poculata* are not expelled at cold temperatures, as they are during heat-stress bleaching, our results suggest that the benefits provided by *B. psygmophilum* at 15 °C are minimal, as reflected by the skeletal roughness. Utilizing naturally symbiotic and aposymbiotic *A. poculata* as our study system to examine this question allows us to link the diel pattern of biomineralization to coral symbionts in a way that was not possible in studies of obligately symbiotic tropical corals.

In recent decades, tropical corals are experiencing higher occurrences of bleaching events due to anthropogenic climate change. By using *A. poculata* as a model for tropical corals, our results can help predict how bleaching events will impact the underlying skeleton of a coral, even if that coral has recovered from said event, including impacts on the biomechanical properties of the skeleton and susceptibility to bioerosion. We did not address bioerosion in the present study, but we uncovered many observations of bioerosion in the skeleton of *A. poculata*. Future analyses should characterize this prominent bioerosion, because this may have a great impact on the breaking and attachment strength of the skeleton (Moynihan *et al.*, 2021). We also hope to understand the role of bioeroders in the calcification of this coral and to explore the possibility that these organisms are active members of the coral holobiont (Del Campo *et al.*, 2017; Massé *et al.*, 2018).

Acknowledgments

We thank Betsy Gladfelter for her invaluable help throughout this project, through both the knowledge in her literature and in-person guidance. We are grateful to Mayra Sánchez-García for her support throughout this project. We acknowledge the Marine Biological Laboratory Central Microscopy Facility staff for their resources and support, which were essential to this project. This work was supported by the Marine Biological Laboratory and the University of Chicago Metcalf program and by a National Institutes of Health Research Project Grant (grant R01EB26300 to PJLR).

Data Accessibility

All data and code, including all images and masks used in the study, have been deposited in Zenodo (https://zenodo.org/record/4782265#.YblQVX3MLa0).

Literature Cited

Al-Horani, F. A., É. Tambutté, and D. Allemand. 2007. Dark calcification and the daily rhythm of calcification in the scleractinian coral, *Galaxea fascicularis*. *Coral Reefs* **26:** 531–538.

Allemand, D., C. Ferrier-Pagès, P. Furla, F. Houlbrèque, S. Puverel, S. Reynaud, É. Tambutté, S. Tambutté, and D. Zoccola. 2004. Biomineralisation in reef-building corals: from molecular mechanisms to environmental control. *C. R. Palevol.* **3:** 453–467.

Allemand, D., É. Tambutté, D. Zoccola, and S. Tambutté. 2011. Coral calcification, cells to reefs. Pp. 119–150 in *Coral Reefs: An Ecosystem in Transition*, Z. Dubinsky and N. Stambler, eds. Springer, Dordrecht, The Netherlands.

Baker, D. M., C. J. Freeman, J. C. Y. Wong, M. L. Fogel, and N. Knowlton. 2018. Climate change promotes parasitism in a coral symbiosis. *ISME J.* **12:** 921–930.

Barnes, D. J., and C. J. Crossland. 1980. Diurnal and seasonal variations in the growth of a staghorn coral measured by time-lapse photography. *Limnol. Oceanogr.* **25:** 1113–1117.

Bertucci, A., S. Forêt, E. E. Ball, and D. J. Miller. 2015. Transcriptomic differences between day and night in *Acropora millepora* provide new insights into metabolite exchange and light-enhanced calcification in corals. *Mol. Ecol.* **24:** 4489–4504.

Bhattacharya, D., S. Agrawal, M. Aranda, S. Baumgarten, M. Belcaid, J. L. Drake, D. Erwin, S. Foret, R. D. Gates, D. F. Gruber *et al.* 2016. Comparative genomics explains the evolutionary success of reef-forming corals. *eLife* **5:** e13288.

Burton, E. A., and L. M. Walter. 1987. Relative precipitation rates of aragonite and Mg calcite from seawater: temperature or carbonate ion control? *Geology* **15:** 111–114.

Chan, A. N., L. A. González-Guerrero, R. Iglesias-Prieto, E. M. Burmester, R. D. Rotjan, J. R. Finnerty, and I. B. Baums. 2021. An algal symbiont (*Breviolum psygmophilum*) responds more strongly to chronic high temperatures than its facultatively symbiotic coral host (*Astrangia poculata*). *bioRxiv*, 2021.02.08.430325.

Chinander, M. R., M. L. Giger, J. M. Martell, C. Jiang, and M. J. Favus. 1999. Computerized radiographic texture measures for characterizing bone strength: a simulated clinical setup using femoral neck specimens. *Med. Phys.* **26:** 2295–2300.

Clode, P. L., and A. T. Marshall. 2004. Calcium localisation by X-ray microanalysis and fluorescence microscopy in larvae of zooxanthellate and azooxanthellate corals. *Tissue Cell* **36:** 379–390.

Cohen, A. L., and T. A. McConnaughey. 2003. Geochemical perspectives on coral mineralization. *Rev. Mineral. Geochem.* **54:** 151–187.

Cohen, A. L., K. E. Owens, G. D. Layne, and N. Shimizu. 2002. The effect of algal symbionts on the accuracy of Sr/Ca paleotemperatures from coral. *Science* **296:** 331–333.

Cohen, I., Z. Dubinsky, and J. Erez. 2016. Light enhanced calcification in hermatypic corals: new insights from light spectral responses. *Front. Mar. Sci.* **2:** 122.

Colombo-Pallotta, M. F., A. Rodríguez-Román, and R. Iglesias-Prieto. 2010. Calcification in bleached and unbleached *Montastraea faveolata*: evaluating the role of oxygen and glycerol. *Coral Reefs* **29:** 899–907.

Del Campo, J., J.-F. Pombert, J. Šlapeta, A. Larkum, and P. J. Keeling. 2017. The "other" coral symbiont: *Ostreobium* diversity and distribution. *ISME J.* **11:** 296–299.

Dimond, J., and E. Carrington. 2008. Symbiosis regulation in a facultatively symbiotic temperate coral: zooxanthellae division and expulsion. *Coral Reefs* **27:** 601–604.

Dimond, J. L., A. H. Kerwin, R. Rotjan, K. Sharp, F. J. Stewart, and D. J. Thornhill. 2013. A simple temperature-based model predicts the upper latitudinal limit of the temperate coral *Astrangia poculata*. *Coral Reefs* **32:** 401–409.

Domart-Coulon, I., J. Stolarski, C. Brahmi, E. Gutner-Hoch, K. Janiszewska, A. Shemesh, and A. Meibom. 2014. Simultaneous extension of both basic microstructural components in scleractinian coral skeleton during night and daytime, visualized by *in situ* ^{86}Sr pulse labeling. *J. Struct. Biol.* **185:** 79–88.

Drake, J. L., T. Mass, J. Stolarski, S. V. Euw, B. van de Schootbrugge, and P. G. Falkowski. 2020. How corals made rocks through the ages. *Glob. Change Biol.* **26:** 31–53.

Falkowski, P. G., Z. Dubinsky, L. Muscatine, and J. W. Porter. 1984. Light and the bioenergetics of a symbiotic coral. *BioScience* **34:** 705–709.

Fitt, W. K., H. J. Spero, J. Halas, M. W. White, and J. W. Porter. 1993. Recovery of the coral *Montastrea annularis* in the Florida Keys after the 1987 Caribbean "bleaching event." *Coral Reefs* **12:** 57–64.

Frankowiak, K., S. Kret, M. Mazur, A. Meibom, M. V. Kitahara, and J. Stolarski. 2016. Fine-scale skeletal banding can distinguish symbiotic from asymbiotic species among modern and fossil scleractinian corals. *PLoS One* **11:** e0147066.

Gattuso, J.-P., D. Allemand, and M. Frankignoulle. 1999. Photosynthesis and calcification at cellular, organismal and community levels in coral reefs: a review on interactions and control by carbonate chemistry. *Am. Zool.* **39:** 160–183.

Gautret, P., J.-P. Cruit, and A. Freiwald. 1997. Composition of soluble mineralizing matrices in zooxanthellate and non-zooxanthellate scleractinian corals: biochemical assessment of photosynthetic metabolism through the study of a skeletal feature. *Facies* **36:** 189–194.

Gladfelter, E. H. 1983. Skeletal development in *Acropora cervicornis* II. Diel patterns of calcium carbonate accretion. *Coral Reefs* **2:** 91–100.

Goreau, T. F. 1959. The physiology of skeleton formation in corals. I. A method for measuring the rate of calcium deposition by corals under different conditions. *Biol. Bull.* **116:** 59–75.

Goreau, T. F., and N. I. Goreau. 1959. The physiology of skeleton formation in corals. II. Calcium deposition by hermatypic corals under various conditions in the reef. *Biol. Bull.* **117:** 239–250.

Gutner-Hoch, E., K. Schneider, J. Stolarski, I. Domart-Coulon, R. Yam, A. Meibom, A. Shemesh, and O. Levy. 2016. Evidence for rhythmicity pacemaker in the calcification process of scleractinian coral. *Sci. Rep.* **6:** 20191.

Heron, S. F., J. A. Maynard, R. van Hooidonk, and C. M. Eakin. 2016. Warming trends and bleaching stress of the world's coral reefs 1985–2012. *Sci. Rep.* **6:** 38402.

Hughes, T. P., A. H. Baird, D. R. Bellwood, M. Card, S. R. Connolly, C. Folke, R. Grosberg, O. Hoegh-Guldberg, J. B. C. Jackson, J. Kleypas *et al.* 2003. Climate change, human impacts, and the resilience of coral reefs. *Science* **301:** 929–933.

Hughes, T. P., K. D. Anderson, S. R. Connolly, S. F. Heron, J. T. Kerry, J. M. Lough, A. H. Baird, J. K. Baum, M. L. Berumen, T. C. Bridge *et al.* 2018. Spatial and temporal patterns of mass bleaching of corals in the Anthropocene. *Science* **359:** 80–83.

Inoue, M., T. Nakamura, Y. Tanaka, A. Suzuki, Y. Yokoyama, H. Kawahata, K. Sakai, and N. Gussone. 2018. A simple role of coral-algal symbiosis in coral calcification based on multiple geochemical tracers. *Geochim. Cosmochim. Acta* **235:** 76–88.

Iwasaki, S., M. Inoue, A. Suzuki, O. Sasaki, H. Kano, A. Iguchi, K. Sakai, and H. Kawahata. 2016. The role of symbiotic algae in the formation of the coral polyp skeleton: 3-D morphological study based on X-ray microcomputed tomography. *Geochem. Geophys. Geosyst.* **17:** 3629–3637.

Jacques, T. G., N. Marshall, and M. E. Q. Pilson. 1983. Experimental ecology of the temperate scleractinian coral *Astrangia danae* II. Effect of temperature, light intensity and symbiosis with zooxanthellae on metabolic rate and calcification. *Mar. Biol.* **76:** 135–148.

Jokiel, P., J. Maragos, and L. Franzisket. 1978. Coral growth: buoyant weight technique. Pp. 529–541 in *Coral Reefs: Research Methods*, D. Stoddart and R. Johannes, eds. UNESCO, Paris.

LaJeunesse, T. C., J. E. Parkinson, and J. D. Reimer. 2012. A genetics-based description of *Symbiodinium minutum* sp. nov. and *S. psygmophilum* sp. nov. (Dinophyceae), two dinoflagellates symbiotic with cnidaria. *J. Phycol.* **48:** 1380–1391.

LaJeunesse, T. C., J. E. Parkinson, P. W. Gabrielson, H. J. Jeong, J. D. Reimer, C. R. Voolstra, and S. R. Santos. 2018. Systematic revision of symbiodiniaceae highlights the antiquity and diversity of coral endosymbionts. *Curr. Biol.* **28:** 2570–2580.

Lentz, S. J., A. L. Cohen, K. E. F. Shamberger, and H. Barkley. 2020. Observations and a model of net calcification declines in Palau's largest coral reef lagoon between 1992 and 2015. *J. Geophys. Res. Oceans* **125:** e2020JC016147.

Li, H., M. L. Giger, O. I. Olopade, A. Margolis, L. Lan, and M. R. Chinander. 2005. Computerized texture analysis of mammographic parenchymal patterns of digitized mammograms. *Acad. Radiol.* **12:** 863–873.

Marshall, A. T. 1996. Calcification in hermatypic and ahermatypic corals. *Science* **271:** 637–639.

Marshall, A. T., and P. Clode. 2004. Calcification rate and the effect of temperature in a zooxanthellate and an azooxanthellate scleractinian reef coral. *Coral Reefs* **23:** 218–224.

Mass, T., H. M. Putnam, J. L. Drake, E. Zelzion, R. D. Gates, D. Bhattacharya, and P. G. Falkowski. 2016. Temporal and spatial expression patterns of biomineralization proteins during early development in the stony coral *Pocillopora damicornis*. *Proc. R. Soc. B Biol. Sci.* **283:** 20160322.

Massé, A., I. Domart-Coulon, S. Golubic, D. Duché, and A. Tribollet. 2018. Early skeletal colonization of the coral holobiont by the microboring Ulvophyceae *Ostreobium* sp. *Sci. Rep.* **8:** 2293.

Moya, A., S. Tambutté, E. Tambutté, D. Zoccola, N. Caminiti, and D. Allemand. 2006. Study of calcification during a daily cycle of the coral *Stylophora pistillata*: implications for "light-enhanced calcification." *J. Exp. Biol.* **209:** 3413–3419.

Moya, A., C. Ferrier-Pagès, P. Furla, S. Richier, E. Tambutté, D. Allemand, and S. Tambutté. 2008. Calcification and associated physiological parameters during a stress event in the scleractinian coral *Stylophora pistillata*. *Comp. Biochem. Physiol. A Mol. Integr. Physiol.* **151:** 29–36.

Moynihan, M. A., S. Amini, N. F. Goodkin, J. T. I. Tanzil, J. Q. I. Chua, G. N. Fabbro, T.-Y. Fan, D. N. Schmidt, and A. Miserez. 2021. Environmental impact on the mechanical properties of *Porites* spp. corals. *Coral Reefs* **40:** 701–717.

Neder, M., P. P. Laissue, A. Akiva, D. Akkaynak, M. Albéric, O. Spaeker, Y. Politi, I. Pinkas, and T. Mass. 2019. Mineral formation in the primary polyps of pocilloporoid corals. *Acta Biomater.* **96:** 631–645.

Pearse, V. B., and L. Muscatine. 1971. Role of symbiotic algae (Zooxanthellae) in coral calcification. *Biol. Bull.* **141:** 350–363.

Peters, E., S. Caims, M. Pilson, J. Wells, W. Jaap, and J. Lang. 1988. Nomenclature and biology of *Astrangia poculata* (= *A. danae*, = *A. astreiformis*) (Cnidaria: Anthozoa). *Proc. Biol. Soc. Wash.* **101:** 234–250.

Rinkevich, B., and Y. Loya. 1984. Does light enhance calcification in hermatypic corals? *Mar. Biol.* **80:** 1–6.

RStudio. 2018. RStudio. Version 1.2.1114. [Online]. RStudio, Boston, MA. Available: http://rstudio.com [2021, August 19].

Sharp, K. H., Z. A. Pratte, A. H. Kerwin, R. D. Rotjan, and F. J. Stewart. 2017. Season, but not symbiont state, drives microbiome structure in the temperate coral *Astrangia poculata*. *Microbiome* **5:** 120.

Spalding, M. D., and B. E. Brown. 2015. Warm-water coral reefs and climate change. *Science* **350:** 769–771.

Sueur, J., T. Aubin, and C. Simonis. 2008. Seewave: a free modular tool for sound analysis and synthesis. *Bioacoustics* **18:** 213–226.

Tambutté, S., M. Holcomb, C. Ferrier-Pagès, S. Reynaud, É. Tambutté, D. Zoccola, and D. Allemand. 2011. Coral biomineralization: from the gene to the environment. *J. Exp. Mar. Biol. Ecol.* **408:** 58–78.

Thornhill, D. J., D. W. Kemp, B. U. Bruns, W. K. Fitt, and G. W. Schmidt. 2008. Correspondence between cold tolerance and temperate biogeography in a western Atlantic *Symbiodinium* (Dinophyta) lineage. *J. Phycol.* **44:** 1126–1135.

van Hooidonk, R., J. Maynard, J. Tamelander, J. Gove, G. Ahmadia, L. Raymundo, G. Williams, S. F. Heron, and S. Planes. 2016. Local-scale projections of coral reef futures and implications of the Paris Agreement. *Sci. Rep.* **6:** 39666.

Von Euw, S., Q. Zhang, V. Manichev, N. Murali, J. Gross, L. C. Feldman, T. Gustafsson, C. Flach, R. Mendelsohn, and P. G. Falkowski. 2017. Biological control of aragonite formation in stony corals. *Science* **356:** 933–938.

Walt, S. van der, J. L. Schönberger, J. Nunez-Iglesias, F. Boulogne, J. D. Warner, N. Yager, E. Gouillart, and T. Yu. 2014. scikit-image: image processing in Python. *PeerJ* **2:** e453.

Appendix

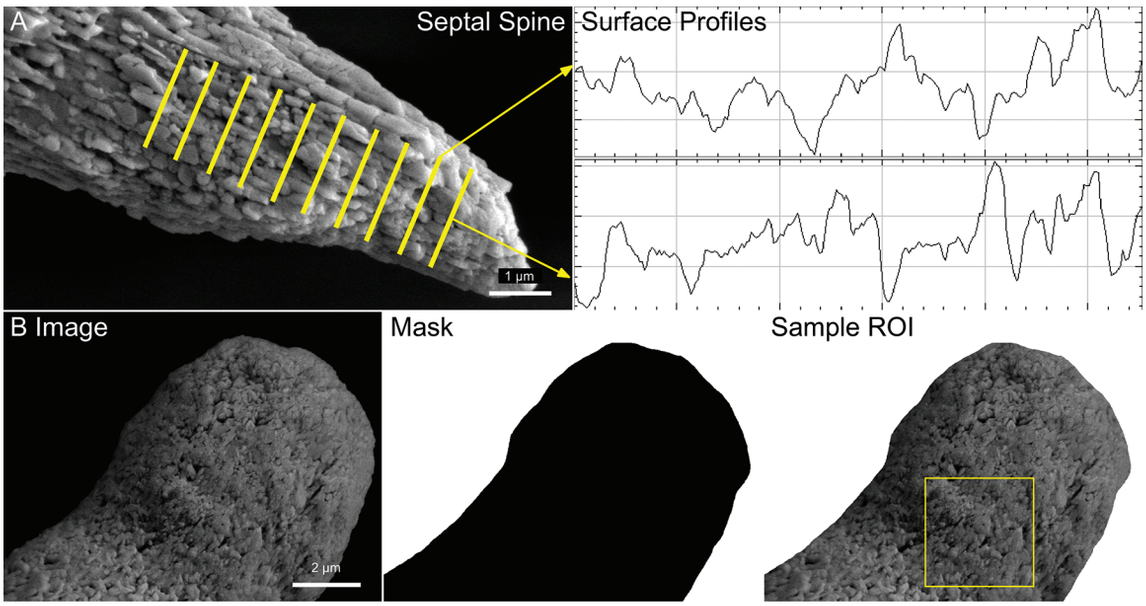

Figure A1. Illustration of image analysis techniques. (A) Method for using surface profiles to quantify the roughness of a surface in scanning electron microscopy (SEM) images of the *Astrangia poculata* skeleton. Ten line segments perpendicular to the axis of the spine are sampled from each image. For each line segment, a surface profile is measured, which is then used for roughness analysis. (B) Illustration of sampling of regions of interest (ROIs) for Fourier transform analysis. For each image, a mask is created to demarcate the spine area. Within the mask, 200 pixel × 200 pixel ROIs (highlighted in yellow) are sampled. The number of ROIs sampled varies depending on the size and geometry of the mask. The first moment of the power spectrum (FMP) was calculated for each ROI by using a two-dimensional Fourier transform.

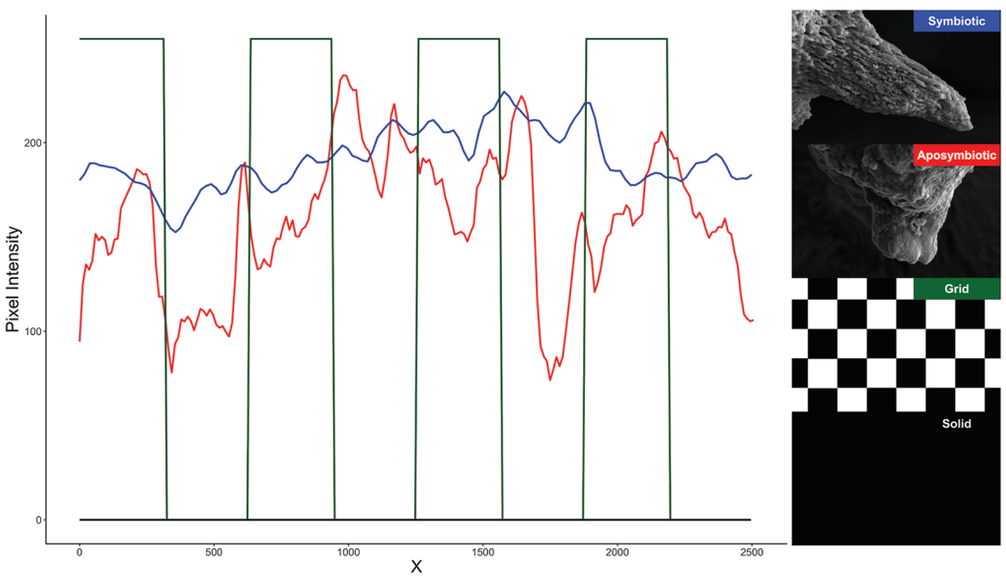

Figure A2. Demonstration of surface profile roughness method. One sample surface profile has been sampled from each image on the left and plotted. These surface profiles resulted in the following roughness measurements: 1047 (symbiotic 27 °C), 16,103 (aposymbiotic 27 °C), 910,350 (grid), and 0 (solid).

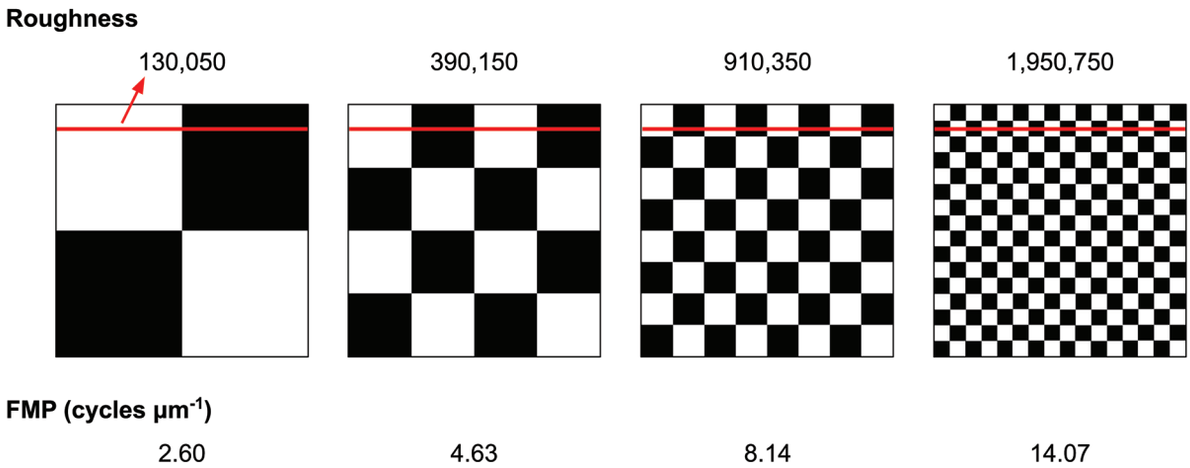

Figure A3. Comparison of roughness and first moment of the power spectrum (FMP) (Li *et al.*, 2005) methods of image analysis. The novel roughness method developed for this study utilizes line segments (red) rather than the whole image, as in the FMP method. The roughness method allows for analysis of the amplitude of the surface profile of the line segment. The FMP method measures the textural frequency of the image.